Ionic conductivity in LixTaOy thin films grown by atomic layer deposition

Hu, Yang

2020-11-20

Hu , Y , Miikkulainen , V , Mizohata , K , Norby , T , Nilsen , O & Fjellvåg , H 2020 , ' Ionic conductivity in LixTaOy thin films grown by atomic layer deposition ' , Electrochimica Acta , vol. 361 , 137019 . https://doi.org/10.1016/j.electacta.2020.137019

http://hdl.handle.net/10138/321240
https://doi.org/10.1016/j.electacta.2020.137019

Electrochimica Acta 361 (2020) 137019

Contents lists available at ScienceDirect

Electrochimica Acta

journal homepage: www.elsevier.com/locate/electacta

Research Paper

Ionic conductivity in Li_xTaO_y thin films grown by atomic layer deposition

Yang Hu[a,*], Ville Miikkulainen[a], Kenichiro Mizohata[b], Truls Norby[a], Ola Nilsen[a], Helmer Fjellvåg[a]

[a] Centre for Materials Science and Nanotechnology, Department of Chemistry, University of Oslo, P.O. Box 1126, Blindern, NO-0318 Oslo, Norway
[b] Division of Materials Physics, Department of Physics, FI-00014 University of Helsinki, Finland

ARTICLE INFO

Article history:
Received 28 June 2020
Revised 19 August 2020
Accepted 25 August 2020
Available online 31 August 2020

Keywords:
Atomic layer deposition
Li_xTaO_y thin films
Solid-state electrolytes
TOF-ERDA
Ionic conductivity

ABSTRACT

The material system Li-Ta-O is a promising candidate for thin-film solid-state electrolytes in Li-ion batteries. In the present study, we have varied the Li content x in Li_xTaO_y thin films grown by atomic layer deposition (ALD) with the aim of improving the Li-ion conductivity. The amorphous films were grown at 225 °C on insulating sapphire and on conductive Ti substrates using tantalum ethoxide ($Ta(OEt)_5$), lithium tert-butoxide (LiO^tBu) and water as reactants. The film composition was determined by time-of-flight elastic recoil detection analysis (TOF-ERDA), displaying an almost linear relationship between the pulsed and deposited Li content. The ionic conductivities were determined by in-plane and cross-plane AC measurements, exhibiting an Arrhenius-type behaviour and comparatively weak thickness-dependence. Increasing Li content x from 0.32 to 0.98 increases the film conductivity by two orders of magnitude while higher Li content $x = 1.73$ results in decreased conductivity. A room-temperature conductivity σ_{RT} of ~10^{-8} S cm^{-1} is obtained for a 169 nm thick $Li_{0.98}TaO_y$ film. The evolution of conductivity and activation energy suggests a competing effect between the concentration and the mobility of mobile Li ions when more Li are incorporated. The compositional dependence of Li transport mechanism is discussed.

1. Introduction

Solid-state batteries are considered the next-generation battery technology, promising lower cost, higher performance and increased safety. By replacing liquid electrolytes with solid counterparts, one eliminates possible release of flammable and poisonous gas, enables thinner electrolytes with higher conductivities, allows for compact designs, and permits the utilization of high-voltage cathodes and even metallic Li anodes to improve the energy and power densities [1]. Currently, the major bottleneck for the realization of solid-state batteries is to identify an appropriate solid electrolyte with adequate Li-ion conductivity and good chemical/electrochemical stability. The low ionic conductivity in solid electrolytes can be compensated by utilizing a thin-film design that can geometrically reduce the internal resistance [2–4], particularly for three-dimensional (3D) microbattery designs [1,5]. One of the most crucial steps in the fabrication of 3D microbatteries is to deposit a conformal and pinhole-free electrolyte thin film. Atomic layer deposition (ALD) has already demonstrated its potential for Li-containing materials and holds promise for enabling such 3D microbatteries. ALD is based on sequential self-limiting gas-solid surface reactions, and it offers high-aspect-ratio conformity, precise thickness control at the angstrom level, tunable composition and freedom in the degree of crystallinity. Additionally, ALD processes are easy to scale up for industry-level applications [6,7].

Since the first report on the deposition of Li-containing films [8], ALD has developed rapidly and become an effective method to synthesize active electrode materials of Li-ion batteries and to engineer the electrode-electrolyte interface for improving the electrode stability and battery cyclability [9–12]. More significantly, ALD has progressively demonstrated its potential to fabricate solid-state electrolytes, which hold the key for the advancement of solid-state batteries and 3D microbatteries. Aaltonen *et al.* [13] firstly suggested ALD grown [(Li, La)$_x$Ti$_y$O$_z$, LLT] amorphous thin films for the application of solid electrolytes. Thereafter, successful depositions of ALD thin-film electrolytes have been reported for various material systems including Li_2O-Al_2O_3 [9,14,15], Li_xTaO_y [16], $Li_{2.8}PO_z$ [17], Li_2O-SiO_2 [18], $Li_7La_3Zr_2O_{12}$ [19], $Li_xAl_ySi_zO$ [20] and

* Corresponding author.
E-mail address: yang.hu@smn.uio.no (Y. Hu).

https://doi.org/10.1016/j.electacta.2020.137019

LiPON [21,22]. Following the primary efforts to develop suitable ALD processes for these materials, the current focus is to optimize their Li-ion conductivity. For a given material system, increasing the Li content in the deposited films is expected to improve the Li-ion conductivity. However, the conductivity characterization of ALD thin films has proven to be challenging because the experimental results are highly dependent on the film thickness and measurement configuration (in-plane [23,24] or cross-plane [25,26]), in addition to the materials chemistry and structure.

In our previous work on $Li_{0.86}AlO_y$ films [15], we found that the cross-plane conductivity provided more reliable information and was less dependent on film thickness. The room-temperature conductivity (σ_{RT}) of ~10^{-10} S cm^{-1} is very different from the values reported for a $Li_{1.6}AlO_y$ films (9×10^{-4} S cm^{-1} at 400°C) [9] and for a thinner Li_xAlO_y film (50 nm, extrapolated σ_{RT} ~5.6×10^{-8} S cm^{-1}) [14], which were both measured by in-plane at higher temperature. Due to the differences in composition, thickness and characterization methods in those works, it is not straightforward which factors are responsible for the significant conductivity deviation. Perng *et al.* [20] investigated a more complex ALD $Li_xAl_ySi_zO$ system and reported that the cross-plane σ_{RT} of ultra-thin films (8 nm) increased from 10^{-9} to close to 10^{-7} S cm^{-1} when Li content *x* increased from *ca.* 0.05 to 0.48. However, they also observed a conductivity decrease by almost two orders of magnitude for a given composition when the film thickness doubled (from 6 to 12 nm). Liu *et al.* [16] deposited Li_xTaO_y films with a large variation in Li stoichiometry (x = 0.6 ~ 12.3) and reported a σ_{RT} of 2×10^{-8} S cm^{-1} for $Li_{5.1}TaO_y$. Recently, Kozen *et al.* [21] deposited LiPON by ALD and obtained conductivities of $1.45–3 \times 10^{-7}$ S cm^{-1} (for N contents 1.8 ~ 16.3%) by investigating a LiPON/organic liquid electrolyte/Li coin cell. Their results are in agreement with the later work on $Li_{0.95}PO_{3.00}N_{0.6}$ film from Nisula *et al.* [22], who reported a conductivity of 6.6×10^{-7} S cm^{-1} at 25°C measured by the cross-plane method. These reports evidenced the feasibility of optimizing the Li conductivity by tuning deposition features and taking advantage of the compositional flexibility of ALD. It has been shown that a small change in the film composition, especially the Li stoichiometry, can lead to a conductivity change by orders of magnitude. However, we can hardly discard the possibility of over- or underestimation when experimental parasitic current cannot be excluded from the thin-film conductivity measurement. Most importantly, it is crucial to accurately determine the film composition in order to evaluate how the ratio of Li pulses influences the actual Li content in the deposited film and thereby the conductivity.

In the present work, we deposited Li_xTaO_y thin films by ALD and studied the relation between their conductivities and compositions. The Li pulsing ratio was gradually increased to obtain higher Li content in the product. Such amorphous films were grown on insulating and on conducting substrates to enable the respective in-plane and cross-plane conductivity measurement. Time-of-flight elastic recoil detection analysis (TOF-ERDA) was used to determine the chemical composition and the element depth profile. Li-ion conductivity was characterized by impedance spectroscopy, and the pre-exponential factor and activation energy were extracted from temperature-dependent measurements. In-plane and cross-plane studies were carried out and compared to assess any effects of thickness dependence. The transport mechanism was discussed based on the conductivity evolution as a function of Li content.

2. Experimental

Li-Ta-O thin films, denoted as Li_xTaO_y, were deposited by ALD onto conducting Ti (ASTM, Astrup AS), insulating sapphire (α-Al_2O_3(0001), University Wafer) and Si(111) (Coating And Crystal Technology Inc.) substrates. Depositions were made with an ASM F-120 Sat reactor at 225 °C. Tantalum ethoxide ($Ta(OEt)_5$) was used as the Ta precursor and held at an evaporation temperature of 100 °C. Lithium tert-butoxide (LiO^tBu) was used as the Li precursor sublimed at 130 °C. Both precursors were delivered using internal sources and inert gas valves. Deionized water, evaporated at room temperature from an external vessel, was used as the oxygen source for both $Ta(OEt)_5$ and LiO^tBu. Depositions of Li_xTaO_y films were conducted using a pulsing sequence of $N\bullet\{A\bullet[LiO^tBu(4\text{-s pulse}/5\text{-s purge}) + H_2O(0.5/5)] + B\bullet[Ta(OEt)_5(3–15/5) + H_2O(0.5/5)]$. Here *A* and *B* denote the number of Li and Ta pulses in the respective Li and Ta subcycle, and $N\bullet\{A+B\}$ is the total number of binary cycles. The Li content in the grown films was controlled by tailoring the ratio between Li and Ta pulses using *A*:*B* = 1:10, 1:6, 1:2 and 1:1. These pulsing schemes will be referred to as 9, 14, 33 and 50% Li pulses in the present work, respectively, based on *A/(A+B)*. Likewise, the ratio of measured Li in the deposited films will be referred to a % Li content based on the cation composition Li/(Li+Ta), in order to distinguish from the Li content *x* corresponding to the Li stoichiometry in Li_xTaO_y. The deposition process is similar to the one reported by Liu *et al.*[16].

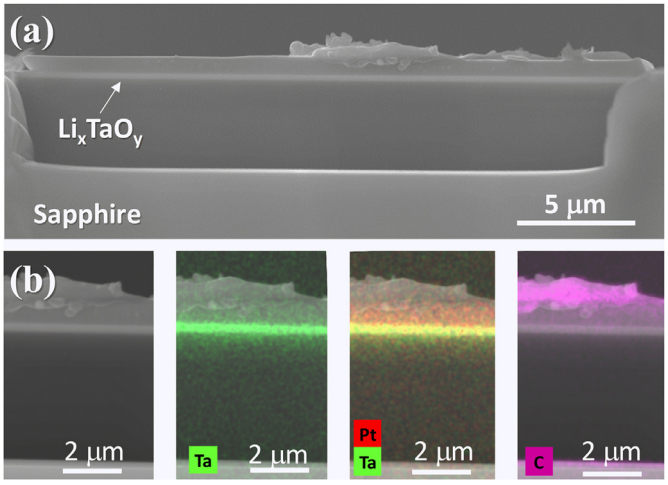

Fig. 1. Cross-section SEM/EDX of the $Li_{0.32}TaO_y$ film (green) on sapphire substrate with Pt electrode (red). Carbon (violet) is the residue from the FIB cutting.

The film thickness was determined by spectroscopic ellipsometry (J.A. Woollam Alpha-SE) using the reference films on Si substrates and the Cauchy function for fitting. The as-grown films were amorphous as determined by XRD (Bruker AXS D8) showing featureless XRD patterns. The elementary composition was characterized by TOF-ERDA, utilizing a 40 MeV $^{127}I^{7+}$ beam. The measurement geometry was 14+26° (incident angle 14° from sample surface, recoil/detection angle 26°).

The Li-ion conductivity was characterized by impedance spectroscopy. Electrode of 100 nm Pt with a 5 nm Ti adhesion layer was deposited using E-beam evaporation (Leybold DC V 6–12 kV). Fig. 1 shows the electrode/film structure of a film on sapphire substrate using the cross section cut by Focused Ion Beam (FIB, FEI Helios NanoLab) and characterized by SEM/EDX (HITACHI SU8230 – Bruker Quantax). Parallel strip electrodes were used for the films grown on sapphire substrates and the conductivity was measured in-plane. Circular electrodes with a diameter of 3 mm were deposited onto the films grown on Ti substrates, and the conductivity was measured cross-plane between the Pt electrode and the Ti substrate. Au wires were attached to the Pt electrodes by Ag paste (ALDRICH, 735825-25G) to ensure a soft contacting. The assembly was mounted in a ProboStat sample holder (NorECs, Norway) with a heating mantle. The conduction characteristics of the film was first verified by measuring the DC resistance with a multimter. The reading of the resistance kept increasing until be-

Table 1
Growth, thickness and composition of Li_xTaO_y films.

% Li pulses	*N* {*A*+*B*}	Growth per binary cycle (Å)	Film thickness (nm)	Formula determined by TOF-ERDA
9 %	2970	0.67	199	$Li_{0.32}TaO_y$
14 %	2800	0.63	175	$Li_{0.51}TaO_y$
33 %	2100	0.80	169	$Li_{0.98}TaO_y$
50 %	1820	0.65	120	$Li_{1.73}TaO_y$

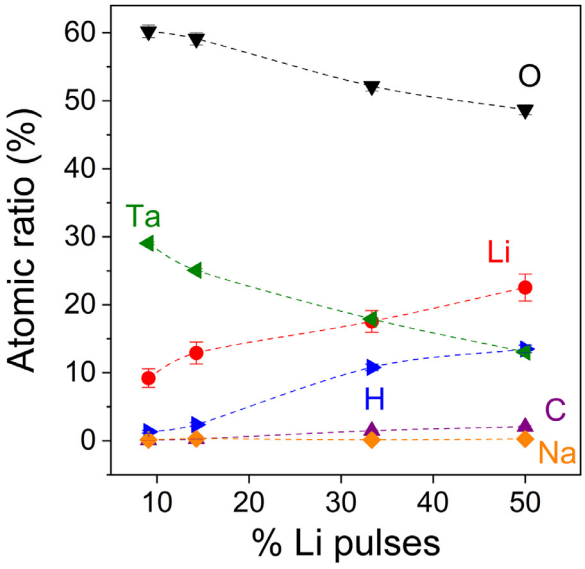

Fig. 2. Elementary composition (atomic ratios by TOF-ERDA) for the films deposited using different %Li pulses

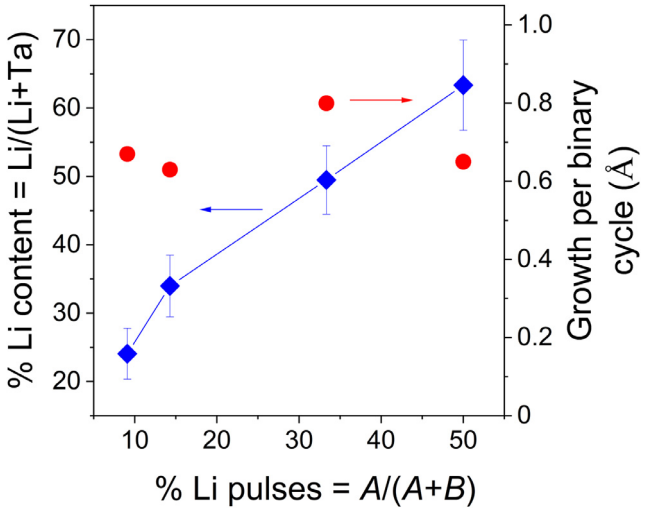

Fig. 3. Variation of the deposited % Li content Li/(Li+Ta) (♦) and the film growth per binary cycle (•) as a function of the % Li pulses *A*/(*A*+*B*).

yond the range, reflecting the ion-blocking effects and evidencing the predominating ionic conduction. The impedance was measured in dry Ar from room temperature (RT) to *ca.* 200 °C (Novocontrol Alpha-A + POT/GAL 15 V 10 A, Novocontrol Technologies) over a frequency range 1 MHz–0.05 Hz with an AC amplitude of 50 mVrms (root-mean-square voltage). For in-plane measurement, data from the first heating were neglected to remove the errors introduced by the surface-adsorbed water [15]. The Li-ion conductivity was calculated from the measurement geometry and the resistances obtained by fitting the impedance data using equivalent circuits (*ZView2*, Scribner Associates Inc.). Further details can be found elsewhere [15].

3. Results and discussion

The elementary composition of as-deposited Li_xTaO_y films analysed by TOF-ERDA is shown in Fig. 2. The increasing Li pulsing ratio leads to a higher Li atomic ratio in the deposited film. However, larger amount of hydrogen and slightly increased carbon are also noticed, especially for the highest 50% Li pulses. This implies that a certain amount of Li is most probably bonded as Li(OH) that could lead to the formation of Li_2CO_3 upon exposure to air. The respective chemical formula is determined through the atomic ratio of elements, denoted as $Li_{0.32}TaO_y$, $Li_{0.51}TaO_y$, $Li_{0.98}TaO_y$ and $Li_{1.73}TaO_y$, which are summarized in Table 1 together with the deposition parameters and the film thickness.

Fig. 3 depicts the % Li content (♦) and the growth per ALD binary cycle (•) as a function of % pulsed Li. In response to the increasing Li pulsing ratio, the pulse time of $Ta(OEt)_5$ has been extended in the present work, which is necessary to ensure the film uniformity. The depositions using a 3 s pulse of $Ta(OEt)_5$ enabled obtaining uniform films for both 9% and 14% Li pulses, but 33% Li pulse resulted in a milky and non-uniform film that was significantly thicker than expected. When the $Ta(OEt)_5$ pulse was extended to 6 s, the film grew again uniformly. Furthermore, a longer 15 s pulse of $Ta(OEt)_5$ was indispensable to achieve uniform film for the highest 50% Li pulse. This effect is similar to what has been reported for the $Li_xTi_yO_z$ ALD process based on LiO^tBu, $Ti(O^iPr)_4$ and water precursors [27]. There, an extended $Ti(O^iPr)_4$ pulse was required to obtain uniform films with higher Li pulsing ratio. Otherwise, the surface could remain unsaturated for too short $Ti(O^iPr)_4$ pulses, resulting in an insufficient precursor dose. Usually in such cases, the deposited films become thinner than expected. However, if the deposited material contains Li, unsaturated $Ti(O^iPr)_4$ or $Ta(OEt)_5$ surface may leave behind a Li-rich surface that is highly hygroscopic. The deposited hygroscopic precursors/products may act as a water reservoir during the subsequent pulse of water that obstructs the self-limiting growth and results in thicker and nonuniform films. Findings within these two similar processes also suggest that titanium and tantalum alkoxide-surface reactions are slower with lithium-containing surfaces since longer pulses are required than in the case of binary oxides without Li. In the present work, it was not possible to obtain uniform films using higher than 50% Li pulse with 15 s $Ta(OEt)_5$ pulses. We did not extend the attempts into even longer $Ta(OEt)_5$ pulse time due to practical reasons.

The variation in deposited % Li content (♦) with % Li pulses (*A*/(*A*+*B*)) follows a scheme that has previously been observed for Na, K, and Rb [28]. The % Li content increases faster when using lower % Li pulses (9 %–14 %), compared to a slower regime where higher % Li pulses (14 %–50 %) were applied. Nevertheless, a linear increase of the deposited content is evident throughout the complete pulsing range. This is in contrast to the Na, K and Rb systems mentioned above, where a reservoir effect was clearly observed at high alkaline contents, with quite abrupt variations. The lack of such features in the present work indicates that the adopted increase in $Ta(OEt)_5$ pulse time is an efficient approach for mitigating

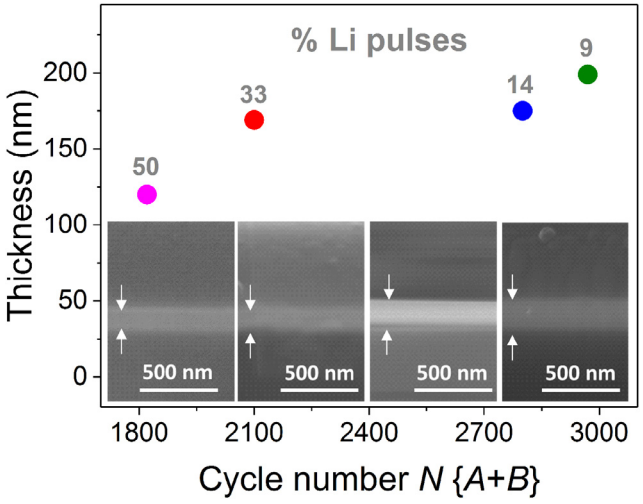

Fig. 4. Thickness of Li_xTaO_y thin films (determined by ellipsometry) against the ALD binary cycle number. Insets are the cross-sectional SEM images of films on sapphire substrate.

such reservoir effects and thereby enables control of the Li content to relatively high levels.

We obtained a growth per binary cycle between 0.63 and 0.80 Å for the % Li pulses up to 33%. These values are in good agreement with the previous work by Liu *et al.* [16], reporting a growth-per-supercycle values of 7.3 and 5.2 Å for 9% and 14% Li pulses, which correspond to 0.66 and 0.74 Å growth per binary cycle, respectively [16]. However, our growth per binary cycle for 50% Li pulse, which is 0.65 Å, is notably lower than their reported value of 1.1 Å (i.e. 2.2 Å per supercycle). This is probably related to our longer $Ta(OEt)_5$ pulse time which seemingly reduced the reservoir effects. Fig. 4 shows the film thickness with varying % Li pulses and cycle number. The thickness measured by ellipsometry using films on Si substrate exhibits good agreement with the cross-sectional SEM observation of films deposited on sapphire substrate.

The depth profile of the $Li_{1.73}TaO_y$ film (Fig. 5) reveals that the elements are uniformly distributed, except in the near-surface region where increased Li, H and C contents are detected. This is likely due to the high mobility of Li, as previously reported for similar Li-ALD processes [27,29]. Liu *et al.* [16] reported considerably higher Li contents for 14% and 50% Li pulses ($Li_{5.1}TaO_y$ and $Li_{12.3}TaO_y$, respectively), determined by X-ray photoelectron spectroscopy (XPS). This may be related to their prominent higher growth rates due to the above-mentioned reservoir effects. It is questionable whether these excess Li enter into the Li_xTaO_y structure, or form an individual amorphous network near the surface.

The Li-ion conductivity is determined by impedance spectroscopy. Fig. 6 (a) displays the Nyquist plots of impedance measured for a 175 nm $Li_{0.51}TaO_y$ film (sapphire substrate, in-plane method) at high temperatures. The impedance spectra consist of a high-frequency semicircle reflecting the film bulk, and a low-frequency inclined line that typically represents the blocking electrode and is an indication of predominantly ionic conductivity [30–32]. A simplified equivalent circuit included in the figure was used to resolve the impedance data: R_b represents the film bulk resistance followed by a capacitive constant phase element CPE_e from the blocking electrode. The film being very thin, its geometrical capacitance is small and masked by the stray capacitance CPE_{stray} mostly from the substrate [33,34]. By using the cross-plane method, on the other hand, the impedance spectra comprise a depressed high-frequency semicircle representing the film bulk overlapping with a low-frequency electrode response, as shown in Fig. 6 (b). The corresponding equivalent circuit includes a film bulk resistance R_b in parallel with a geometrical capacitance CPE_g of the film, which is large enough to be distinguished, together followed in series by the capacitive contribution CPE_e of the blocking-electrode. The ionic conductivities are calculated from the film bulk resistances R_b, and the length and area of the respective conduction pathway.

The Li-ion conductivities as a function of temperature are shown in Fig. 7. Both in-plane and cross-plane conductivities increase gradually with the Li content x from 0.32 to 0.98, but the $Li_{1.73}TaO_y$ film with the highest Li content shows lower conductivities than $Li_{0.51}TaO_y$ and $Li_{0.98}TaO_y$ at the temperature below 100°C. It is worth noting that for the very same film, the in-plane conductivities are almost one order of magnitude higher than the cross-plane ones. We previously compared these two methods for $LiAlO_2$ films with the same composition but different thickness (90, 160 and 235 nm) [15], and found a moderate thickness-dependence of in-plane conductivity while a better agreement was achieved for cross-plane conductivity. In the present work, the Li_xTaO_y films have both compositional variation and thickness difference, but the latter is comparatively small (~ 80 nm). Moreover, the film thicknesses (120–199 nm) are far beyond the "ultra-thin" regions, where the assessment of in-plane conductivity can be significantly influenced by the structural modulation or the hetero-interface effect [35,36]. Therefore, for the present study we acknowledge the conductivity deviation introduced by the different measurement configuration and the thickness-dependence, but consider the compositional factor, namely the Li content, is prevailing.

The conductivity evolution exhibits a thermally activated mechanism and follows the Arrhenius-type relation for diffusing species: $\sigma T = \sigma_0 \exp(-E_a/kT)$. Here E_a denotes the activation energy, k is Boltzmann's constant, T is the absolute temperature, and σ_0 is the pre-exponential factor that can be related to the migration entropy, jump frequency, attempt frequency and geometry factor and so on when a simple uncorrelated hopping mechanism is considered. The fitted E_a and σ_0 together with the room-temperature conductivity σ_{RT} are listed in Table 2.

The evolution of σ_{RT}, σ_0 and E_a upon Li content x is illustrated in Fig. 8. Both in-plane and cross-plane σ_{RT} increase by nearly two orders of magnitude from $x = 0.32$ to $x = 0.98$ and then drastically decrease at the highest Li content $x = 1.73$. The increase of in-plane conductivity is accompanied by the increasing pre-exponential factor and the reduced activation energy, and σ_{RT}, σ_0 and E_a share the same inflection point at $x = 0.98$. On the other hand, the cross-plan E_a inflects at $x = 0.51$ and has a considerably higher value (~0.76 eV) than the in-plane one (0.64 eV) at $x = 0.98$, suggesting the Li content may influence the transport mechanism in a different way for the films measured by in-plane and cross-plane configuration.

For a single ionic charge carrier i, the macroscopic ionic conductivity (σ_i) can be simply described by the product of the ionic charge ($z_i e$), the charge mobility (μ_i) and the concentration of mobile charge carriers (C_i) as: $\sigma_i = z_i e C_i \mu_i$ [37]. For Li_xTaO_y films in the present study, until $x = 0.98$, we can consider that each mobile Li ion is weakly bonded through the non-bridging-oxygen (NBO) to one $[TaO_6]^-$ octahedron that is corner-linked with one another in a random array, and those Li ions hop from one equilibrium NBO site to another [38]. With higher Li content, the amount of mobile charge carriers is increased and more potential jump target sites are introduced, which can reduce the average jump distance as well as the energy barriers for the Li transport [39]. However, in amorphous electrolytes, the cations mobility is intrinsically concentration dependent. Early studies on Li-containing glasses also revealed that the glass conductivity is a result of interplay between the Li concentration and the Li mobility when excess Li is incorporated into the glass matrix, leading to a conductivity maximum at a certain Li cation fraction [38,40–43]. This is in agreement

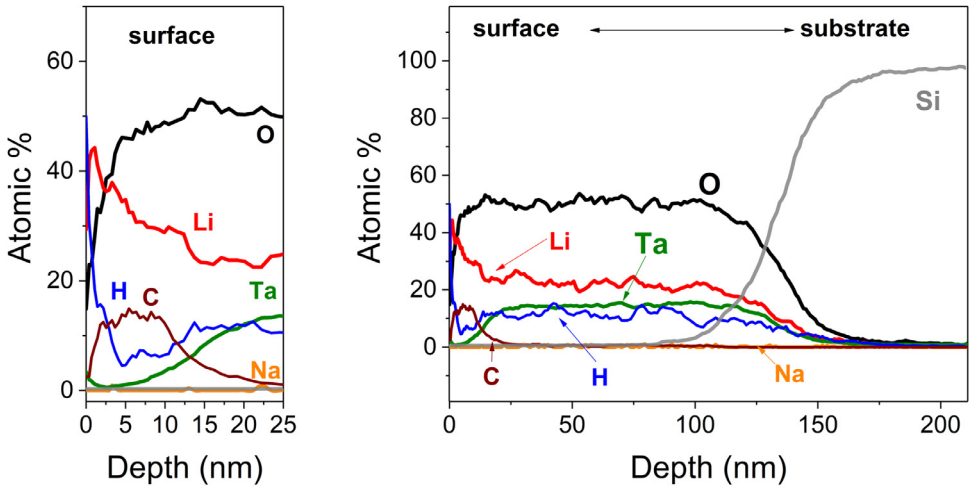

Fig. 5. TOF-ERDA elemental depth profiling of $Li_{1.73}TaO_y$ film. Enlarged view of the near-surface region is shown on the left. Curves have been smoothed using adjacent-averaging for clearer interpretation.

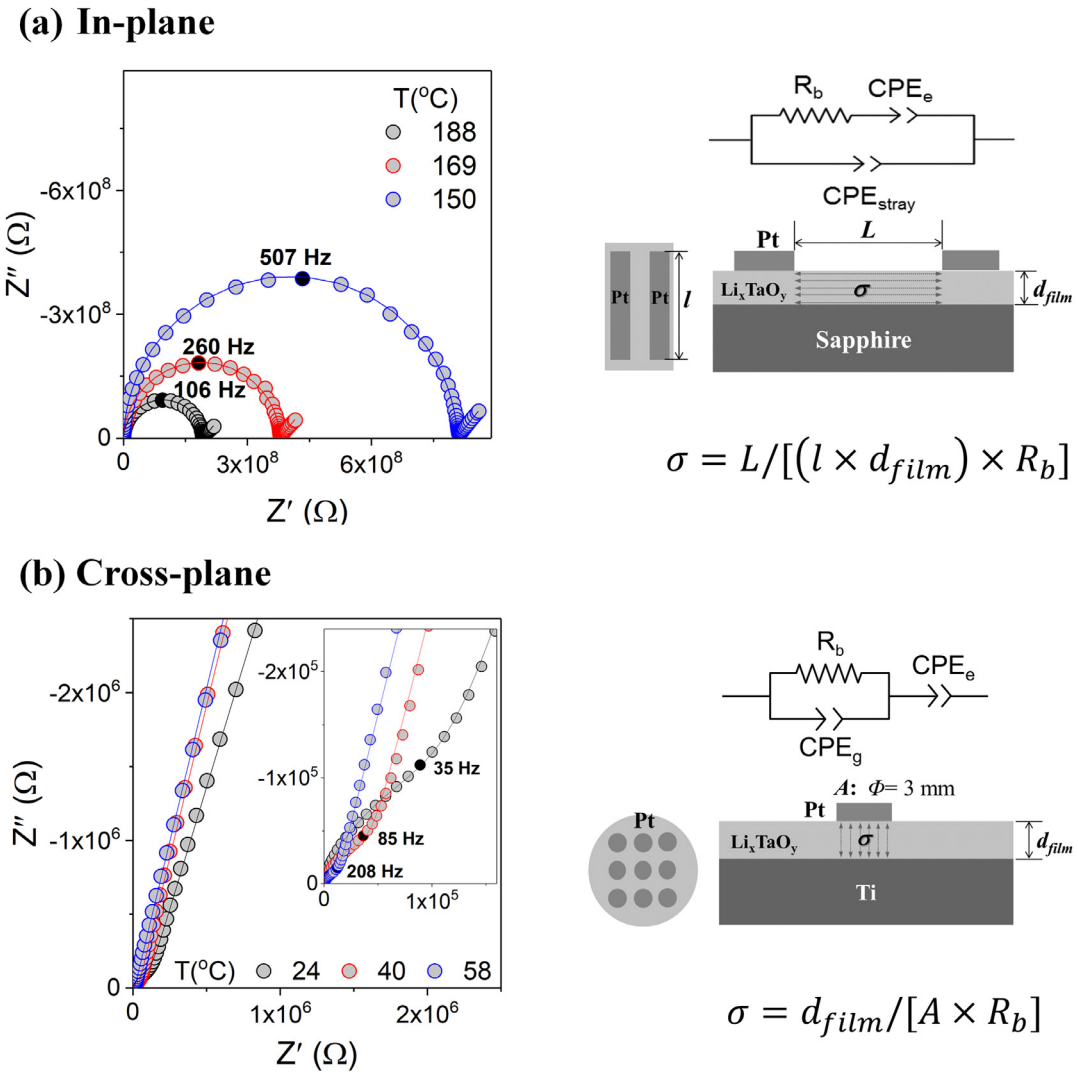

Fig. 6. Impedance spectra of 175 nm $Li_{0.51}TaO_y$ films measured by in-plane (a) and cross-plane (b) methods. Solid lines represent the fitting results using the corresponding equivalent circuits shown on the right.

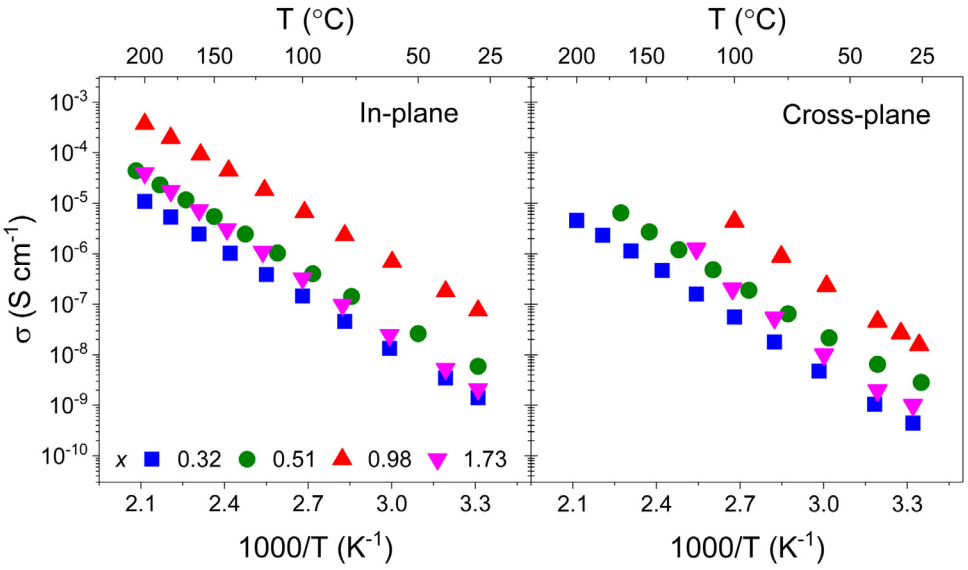

Fig. 7. Conductivity of Li_xTaO_y thin films as a function of temperature measured by in-plane (left) and cross-plane (right) method (in dry Ar). Cross-plane conductivities of $x = 0.98$ and 1.73 at high temperature were not obtained due to short-circuiting.

Table 2
Room-temperature conductivities σ_{RT}, pre-exponential factors σ_0 and activation energies E_a for the Li_xTaO_y films

x in Li_xTaO_y	Thickness (nm)	In-plane			Cross-plane		
		σ_{RT} (S cm^{-1})	σ_0 (S cm^{-1} K)	E_a (eV)	σ_{RT} (S cm^{-1})	σ_0 (S cm^{-1} K)	E_a (eV)
0.32	199	1.4×10^{-9}	7.9×10^{4}	0.68	4.5×10^{-10}	7.2×10^{4}	0.70(1)
0.51	175	6.0×10^{-9}	1.8×10^{5}	0.66	2.9×10^{-9}	9.8×10^{4}	0.65(1)
0.98	169	7.5×10^{-8}	1.3×10^{6}	0.64	1.6×10^{-8}	2.5×10^{7}	0.76(2)
1.73	120	2.1×10^{-9}	1.4×10^{6}	0.74	1.1×10^{-9}	3.2×10^{6}	0.78(3)

Table 3
Comparison of conductivity for Li-Ta-O systems

Materials	Preparation	Determination of composition	σ (S cm^{-1})	E_a (eV)	Ref.
$LiTaO_3$ nanocrystalline	ball-milling		3×10^{-6} (450 K)	0.63(1)	[44]
$Li_{2.57}TaO_y$ films	RF-sputtering	XRD + ICP	8×10^{-8} (300 K)	0.25(1)	[41]
$LiTaO_3$ glass	quenching		~10^{-6} (300 K)	0.38	[43]
$Li_{5.1}TaO_y$ films	ALD	XPS	2×10^{-8} (299 K)	0.55	[16]
$Li_{0.98}TaO_y$ films	ALD	TOF-ERDA	2~8 $\times 10^{-8}$ (300 K)	0.6 ~0.8	this work

with the present work: the highest conductivity is obtained at $x = 0.98$.

Pulsing excess Li into the films, as for $x = 1.73$, introduces more NBOs in the amorphous matrix and weakens the network connectivity, resulting in a more compacted and "close" local environment with limited Li sites and transport pathways. Too many NBOs can also form negatively charged centres that act as Li traps, which has been widely considered limiting factor for the Li ion mobility in those glassy systems [41,42]. These effects can be reflected in the present work by the decreased σ_0 and higher E_a for the cross-plane conductivity when x is increased to 1.73. On the other hand, the in-plane conductivity shows a mild σ_0 change but a pronounced E_a increase (0.64–0.74 eV), indicating the Li transport in these films on sapphire substrate is predominately limited by the increased energy barrier at high Li content. It is also worth noting that σ_{RT}, E_a and σ_0 demonstrate the maximum difference between in-plane and cross-plane results at $x = 0.98$. We therefore assume higher Li concentration may lead to larger local structure difference between the films deposited on sapphire and Ti substrates, and the excess Li limits the macroscopic conductivity in a different way. In addition, as mentioned above, the high H content and the surface enrichment observed in $Li_{1.73}TaO_y$ may form an amorphous mixture of LiOH in the film bulk, where the Li is bounded as Li(OH) instead of to the NBOs and therefor do not contribute to the conductivity. The formation of lithium carbonates on the surface of films with higher Li content, as evidenced by the C enrichment in the near-surface region (Fig. 5), also consumes mobile Li ions and influences the conductivity measurement. Since the Pt contacts are deposited on top of the film surface for both geometry configuration, we anticipate the lithium carbonate to affect the Li transport and contribute to the increase of activation energy for in- and cross-plane conductivity. To prevent such a carbonate layer would require all-inert handling, which was beyond the scope of the present work.

A comparison with previously reported crystalline, amorphous and thin-film Li-Ta-O systems is given in Table 3. The best σ_{RT} of ~10^{-8} S cm^{-1} for the $Li_{0.98}TaO_y$ film in the present work is comparable with what have been reported for the ALD and RF-sputtered films [16,41,43], and the amorphous films exhibit greatly higher conductivity than the crystalline analogues. Despite the conductivity value of the same order of 10^{-8} S cm^{-1}, the reported Li content varies in a large scale (x: 1 ~ 5.1), probably due to the different techniques for composition analysis. Among these reported systems, it is common that the best conductivity is not necessarily obtained with the highest Li content, in consistency with the present work, evidencing the existence of an optimal composition

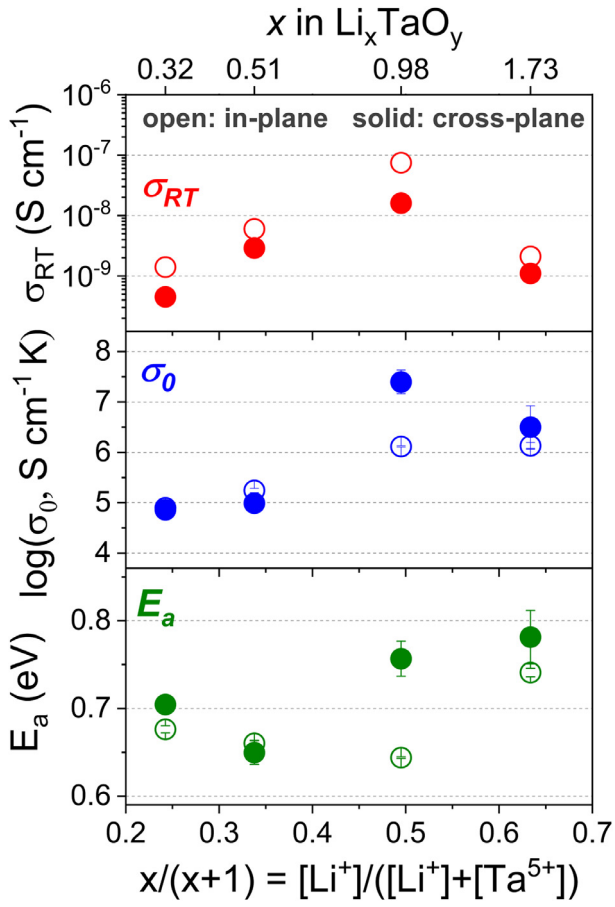

Fig. 8. Compositional dependence of the room-temperature conductivities (σ_{RT}), pre-exponential factor (σ_0) and activation energy (E_a) as a function of the Li cation fraction $x/(x+1)$.Open symbols: in-plane, solid symbols: cross-plane.

with the maximum conductivity. Further investigations on Li_xTaO_y with the composition variation in a narrower range around $x = 1$ can help to understand the conductivity evolution and identify the limiting factors with respect to the deposition process and the film growth mechanism.

4. Conclusions

Li_xTaO_y thin films were deposited by atomic layer deposition utilizing the pulsing sequence N•{A•[LiO^{t}Bu(4-s pulse/5-s purge) + H_2O(0.5/5)] + B•[Ta(OEt)$_5$(3–15/5) + H_2O(0.5/5)]. The films are grown on both insulating sapphire and conductive Ti substrates at 225 °C and exhibit amorphous characteristics. Increasing Li pulsing ratio was applied to achieve higher Li concentration. Ta(OEt)$_5$ pulsing time was gradually extended to overcome the reservoir effects and to ensure the control of Li content in a self-limiting process. Films composition were determined by TOF-ERDA, showing a monotonic increase of deposited Li content upon pulsed Li content. A surface enrichment of Li, H and C was observed in films with higher Li content. The ionic conductivities were determined by both in-plane and cross-plane methods, demonstrating an Arrhenius-type behaviour. Li content proves to be the governing factor for the conductivity: increasing x from 0.32 to 0.98 leads to improved Li-ion conductivity by two orders and a higher Li concentration ($x = 1.73$) results in decreased conductivity. The compositional dependence of Li transport is in agreement with a competing mechanism between the increased Li concentration and the reduced Li mobility. The evolution in activation energy also suggests a different limiting factor for the in-plane and cross-plane conductivity, probably due to the local structure difference resulting from the increased impurity level and the deviated film growth when high Li pulsing ratio is applied. The best σ_{RT} of ~10^{-8} S cm^{-1} is obtained in $Li_{0.98}TaO_y$ film and it shows good agreement with previous reports.

Declaration of Competing Interest

The authors declare that they have no known competing financial interests or personal relationships that could have appeared to influence the work reported in this paper.

CRediT authorship contribution statement

Yang Hu: Methodology, Investigation, Visualization, Writing - original draft. **Ville Miikkulainen:** Methodology, Investigation, Writing - review & editing. **Kenichiro Mizohata:** Methodology. **Truls Norby:** Conceptualization, Supervision, Resources, Writing - review & editing. **Ola Nilsen:** Conceptualization, Resources, Writing - review & editing. **Helmer Fjellvåg:** Resources, Supervision, Funding acquisition.

Funding Sources

This work is financially supported by the Research Council of Norway via projects NanoMILiB (NO. 220135) and 3DBatt (No. 200030).

Acknowledgments

The authors thank our colleagues Dr. A. Evans and Dr. S. Kumar for fruitful discussions and Dr. K. Bergum at UiO MiNaLab for technical assistance of the E-beam deposition. The Research Council of Norway is acknowledged for the support to the Norwegian Micro- and Nano-Fabrication Facility, NorFab (197411/V30).

References

[1] J.F.M. Oudenhoven, L. Baggetto, P.H.L. Notten, All-Solid-State Lithium-Ion Microbatteries, A review of various three-dimensional concepts, Adv. Energy Mater. 1 (2011) 10–33.
[2] J.L. Souquet, M. Duclot, Thin film lithium batteries, Solid State Ion. 148 (2002) 375–379.
[3] N.J. Dudney, Solid-state thin-film rechargeable batteries, Mat. Sci. Eng. B-Solid 116 (2005) 245–249.
[4] S.-J. Lee, H.-K. Baik, S.-M. Lee, An all-solid-state thin film battery using LISIPON electrolyte and Si–V negative electrode films, Electrochem. Commun., 5 (2003) 32–35.
[5] J.W. Long, B. Dunn, D.R. Rolison, H.S. White, Three-dimensional battery architectures, Chem. Rev. 104 (2004) 4463–4492.
[6] O. Nilsen, V. Miikkulainen, K.B. Gandrud, E. Ostreng, A. Ruud, H. Fjellvag, Atomic layer deposition of functional films for Li-ion microbatteries, Phys. Status Solid. A 211 (2014) 357–367.
[7] V. Miikkulainen, M. Leskelä, M. Ritala, R.L. Puurunen, Crystallinity of inorganic films grown by atomic layer deposition: Overview and general trends, J. Appl. Phys. 113 (2013) 021301.
[8] M. Putkonen, T. Aaltonen, M. Alnes, T. Sajavaara, O. Nilsen, H. Fjellvåg, Atomic layer deposition of lithium containing thin films, J. Mater. Chem. 19 (2009) 8767–8771.
[9] T. Aaltonen, O. Nilsen, A. Magrasó, H. Fjellvåg, Atomic layer deposition of Li2O–Al2O3 thin films, Chem. Mater. 23 (2011) 4669–4675.
[10] E. Ostreng, K.B. Gandrud, Y. Hu, O. Nilsen, H. Fjellvag, High power nano-structured V2O5 thin film cathodes by atomic layer deposition, J. Mater. Chem. A 2 (2014) 15044–15051.
[11] J. Xie, J. Zhao, Y. Liu, H. Wang, C. Liu, T. Wu, P.-C. Hsu, D. Lin, Y. Jin, Y. Cui, Engineering the surface of LiCoO2 electrodes using atomic layer deposition for stable high-voltage lithium ion batteries, Nano Res. 10 (2017) 3754–3764.
[12] O. Srur-Lavi, V. Miikkulainen, B. Markovsky, J. Grinblat, M. Talianker, Y. Fleger, G. Cohen-Taguri, A. Mor, Y. Tal-Yosef, D. Aurbach, Studies of the electrochemical behavior of LiNi0.80Co0.15Al0.05O2 Electrodes Coated with LiAlO2, J. Electrochem. Soc. 164 (2017) A3266–A3275.
[13] T. Aaltonen, M. Alnes, O. Nilsen, L. Costelle, H. Fjellvåg, Lanthanum titanate and lithium lanthanum titanate thin films grown by atomic layer deposition, J. Mater. Chem. 20 (2010) 2877–2881.

[14] J.S. Park, X. Meng, J.W. Elam, S. Hao, C. Wolverton, C. Kim, J. Cabana, Ultra-thin Lithium-Ion conducting coatings for increased interfacial stability in high voltage Lithium-Ion Batteries, Chem. Mater. 26 (2014) 3128–3134.
[15] Y. Hu, A. Ruud, V. Miikkulainen, T. Norby, O. Nilsen, H. Fjellvag, Electrical characterization of amorphous LiAlO2 thin films deposited by atomic layer deposition, RSC Adv. 6 (2016) 60479–60486.
[16] J. Liu, M.N. Banis, X.F. Li, A. Lushington, M. Cai, R.Y. Li, T.K. Sham, X.L. Sun, Atomic Layer Deposition of Lithium Tantalate Solid-State Electrolytes, J. Phys. Chem. C 117 (2013) 20260–20267.
[17] W. Biqiong, L. Jian, S. Qian, L. Ruying, S. Tsun-Kong, S. Xueliang, Atomic layer deposition of lithium phosphates as solid-state electrolytes for all-solid-state microbatteries, Nanotechnology 25 (2014) 504007.
[18] B. Wang, J. Liu, M. Norouzi Banis, Q. Sun, Y. Zhao, R. Li, T.-K. Sham, X. Sun, Atomic layer deposited Lithium Silicates as solid-state electrolytes for all–solid-state batteries, ACS Appl. Mater. Interfaces 9 (2017) 31786–31793.
[19] E. Kazyak, K.-H. Chen, K.N. Wood, A.L. Davis, T. Thompson, A.R. Bielinski, A.J. Sanchez, X. Wang, C. Wang, J. Sakamoto, N.P. Dasgupta, Atomic layer deposition of the solid electrolyte garnet Li7La3Zr2O12, Chem. Mater. 29 (2017) 3785–3792.
[20] Y.-C. Perng, J. Cho, S.Y. Sun, D. Membreno, N. Cirigliano, B. Dunn, J.P. Chang, Synthesis of ion conducting LixAlySizO thin films by atomic layer deposition, J. Mater. Chem. A 2 (2014) 9566–9573.
[21] A.C. Kozen, A.J. Pearse, C.-F. Lin, M. Noked, G.W. Rubloff, Atomic layer deposition of the solid electrolyte LiPON, Chem. Mater. 27 (2015) 5324–5331.
[22] M. Nisula, Y. Shindo, H. Koga, M. Karppinen, atomic layer deposition of Lithium Phosphorus Oxynitride, Chem. Mater. 27 (2015) 6987–6993.
[23] S. Sanna, V. Esposito, J.W. Andreasen, J. Hjelm, W. Zhang, T. Kasama, S.B. Simonsen, M. Christensen, S. Linderoth, N. Pryds, Enhancement of the chemical stability in confined [delta]-Bi2O3, Nat. Mater. 14 (2015) 500–504.
[24] E. Navickas, M. Gerstl, G. Friedbacher, F. Kubel, J. Fleig, Measurement of the across-plane conductivity of YSZ thin films on silicon, Solid State Ion. 211 (2012) 58–64.
[25] X. Yu, J.B. Bates, G.E. Jellison, F.X. Hart, A stable thin-film lithium electrolyte: lithium phosphorus oxynitride, J. Electrochem. Soc. 144 (1997) 524–532.
[26] I. Seo, S.W. Martin, Fast lithium ion conducting solid state thin-film electrolytes based on lithium thio-germanate materials, Acta Mater. 59 (2011) 1839–1846.
[27] V. Miikkulainen, O. Nilsen, M. Laitinen, T. Sajavaara, H. Fjellvag, Atomic layer deposition of LixTiyOz thin films, RSC Adv. 3 (2013) 7537–7542.
[28] H.H. Sønsteby, O. Nilsen, H. Fjellvåg, Atomic layer deposition of (K,Na)(Nb,Ta)O3 thin films, J. Vac. Sci. Technol. A 34 (2016) 041508.
[29] E. Ostreng, H.H. Sonsteby, T. Sajavaara, O. Nilsen, H. Fjellvag, Atomic layer deposition of ferroelectric LiNbO3, J. Mater. Chem. C 1 (2013) 4283–4290.
[30] V. Thangadurai, W. Weppner, Li6ALa2Ta2O12 (A=Sr,Ba): Novel Garnet-Like Oxides for Fast Lithium Ion Conduction, Adv. Funct. Mater. 15 (2005) 107–112.
[31] K. Benaissa, P.V. Ashrit, G. Bader, F.E. Girouard, V.-V. Truong, Electrical and optical properties of LiNbO3, Thin Solid Films 214 (1992) 219–222.
[32] V. Thangadurai, R.A. Huggins, W. Weppner, Use of simple ac technique to determine the ionic and electronic conductivities in pure and Fe-substituted SrSnO3 perovskites, J. Power Sources 108 (2002) 64–69.
[33] M. Gerstl, E. Navickas, G. Friedbacher, F. Kubel, M. Ahrens, J. Fleig, The separation of grain and grain boundary impedance in thin yttria stabilized zirconia (YSZ) layers, Solid State Ion. 185 (2011) 32–41.
[34] C. Li, L. Gu, J. Maier, Enhancement of the Li Conductivity in LiF by Introducing Glass/Crystal Interfaces, Adv. Funct. Mater. 22 (2012) 1145–1149.
[35] S.-i. Furusawa, A. Kamiyama, T. Tsurui, Fabrication and ionic conductivity of amorphous lithium meta-silicate thin film, Solid State Ion. 179 (2008) 536–542.
[36] J. Li, N.J. Dudney, J. Nanda, C. Liang, Artificial Solid Electrolyte Interphase To Address the Electrochemical Degradation of Silicon Electrodes, ACS Appl. Mater. Interfaces 6 (2014) 10083–10088.
[37] P.G. Bruce, Solid State Electrochemistry, Cambridge University Press, Cambridge, 2009.
[38] K. Nassau, R.J. Cava, A.M. Glass, The ionic conductivity variation in rapidly quenched lithium-containing glasses, Solid State Ion. 2 (1981) 163–170.
[39] D. Zielniok, C. Cramer, H. Eckert, Structure/Property Correlations in Ion-Conducting Mixed-Network Former Glasses: Solid-State NMR Studies of the System Na2O-B2O3-P2O5, Chem. Mater. 19 (2007) 3162–3170.
[40] P.G. Bruce, Solid state electrochemistry, Cambridge University Press, Cambridge, U.K.; New York, NY, USA, 1997.
[41] L. Zhiyong, C. Xiaofeng, H. Xingfang, The preparation and ionic conductance of nano-amorphous LixTaOy thin film, J. Phys. D: Appl. Phys. 29 (1996) 2740.
[42] A.M. Glass, K. Nassau, Lithium ion conduction in rapidly quenched Li2O-Al2O3, Li2O-Ga2O3, and Li2O-Bi2O3 glasses, J. Appl. Phys. 51 (1980) 3756–3761.
[43] A.M. Glass, K. Nassau, T.J. Negran, Ionic conductivity of quenched alkali niobate and tantalate glasses, J. Appl. Phys. 49 (1978) 4808–4811.
[44] M. Wilkening, V. Epp, A. Feldhoff, P. Heitjans, Tuning the Li diffusivity of poor ionic conductors by mechanical treatment: High Li conductivity of strongly defective LiTaO3 nanoparticles, J. Phys. Chem. C 112 (2008) 9291–9300.